Synthesis, Characterization, DNA Binding Properties, and Solution Thermochromism of Platinum(II) Complexes of the Ethidium Cation: Regiospecificity in a DNA-Promoted Reaction

Tong Ren, Daniel P. Bancroft, Wesley I. Sundquist, Axel Masschelein, Michael V. Keck, and Stephen J. Lippard*

Contribution from the Department of Chemistry, Massachusetts Institute of Technology, Cambridge, Massachusetts 02139

Received June 14, 1993®

Abstract: The reaction of $[Pt(NH_3)_nCl_{4-n}]^{(n-2)}$ (n = 1, 2, and 3) complexes with 1 equiv of the ethidium (Etd) cation afforded *cis*-$[Pt(NH_3)_2(Etd)Cl]^{2+}$, *trans*-$[Pt(NH_3)_2(Etd)Cl]^{2+}$, *cis*-$[Pt(NH_3)(Etd)Cl_2]^{+}$, and $[Pt(NH_3)_3(Etd)]^{3+}$, in which Etd is coordinated to platinum through one of its two exocyclic amino groups. These *N3* and *N8* linkage isomers were separated by reverse-phase HPLC. The platinum coordination sites on ethidium were determined with the use of both ^{195}Pt and ^{1}H NMR spectroscopy as well as by single-crystal X-ray diffraction studies of the *N3* and *N8* isomers of *cis*-$[Pt(NH_3)_2(Etd)Cl]Cl_2$. Solutions of the acetate salts of all the complexes displayed temperature-dependent optical spectroscopic changes in which a transition at ~490 nm (orange) diminished in intensity with concomitant growth of a band at ~640 nm (blue) as the temperature increased. This reversible thermochromic phenomenon was shown to arise from proton transfer between the coordinated exocyclic amino group and the acetate counterion. Temperature-dependent electronic spectral changes resulting from this reaction were fit to the appropriate equilibrium expressions by global analysis, yielding the corresponding thermodynamic parameters, $\Delta H°$ and $\Delta S°$. Acidity constants for the deprotonation of the coordinated exocyclic amino groups were determined from such equilibrium studies of most of the complexes in methanol and converted to the corresponding values in aqueous solution. These experiments revealed the effects of overall charge, linkage isomerism, and platinum geometric isomerism on the pK_a values of the coordinated amino group. Through a Fenske-Hall molecular orbital analysis, the 490-nm band was assigned as a charge-transfer transition from the lone pair orbital of the uncoordinated exocyclic amino nitrogen to the π^* orbital (LUMO) of the phenanthridinium ring. The blue band at ~640 nm was best described as a charge-transfer transition from a π orbital delocalized over the Pt-N(coordinated exocyclic amine) linkage to the π^* orbital of the phenanthridinium ring. The ability to assign the relative pK_a values of the linkage isomers has been used to demonstrate that the previously reported DNA-promoted reaction between *cis*-DDP and ethidium is regiospecific, with the platinum reacting primarily at the *N8* position of the Etd ring.

For more than a decade, *cis*-diamminedichloroplatinum(II) (*cis*-DDP) has been used clinically as a potent anticancer agent against a variety of tumor systems.[1] Correspondingly, there has been intense interest in the coordination chemistry of platinum ammine complexes with nucleobases, oligonucleotides, and DNA.[2] Intercalators, such as ethidium (Etd) bromide, induce changes in both the mode and exonuclease III sensitive sites of binding of *cis*-DDP with DNA, suggesting the occurrence of an intercalator/drug interaction.[3,4] Although *cis*-DDP does not react

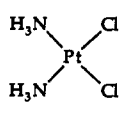

cis-DDP

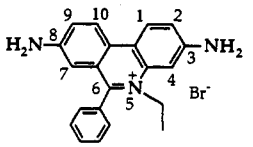

Ethidium Bromide, Etd Br

appreciably with ethidium in dilute (~50 μM) aqueous solution, in the presence of duplex DNA a significant reaction occurs in which a DNA-Pt-ethidium ternary complex is formed.[5-7] The structure of this ternary complex has been elucidated from spectroscopic studies employing model complexes formed in the reaction of *cis*-DDP with Etd in dimethylformamide.[7] In particular, a *cis*-$\{Pt(NH_3)_2\}^{2+}$ moiety bound monofunctionally to DNA, presumably at the *N7* position of either a guanine or adenine nucleobase, is coordinated to one of the amino groups of Etd. In this reaction, DNA serves as a template, facilitating complex formation by holding the reactants in close proximity, resulting in at least a 60-fold increase in the rate of formation of the Pt-Etd bond.[7] Recently, a second example of this type of reaction was reported.[8] In addition to their unique ability to form in a DNA-promoted reaction, platinum ethidium complexes exhibit unusual thermochromism in solution not observed with either *cis*-DDP or ethidium alone. Thermochromism, or the reversible dependence of color on temperature, occurs in a wide variety of both organic and inorganic compounds.[9,10]

Here we present the synthesis and characterization of an expanded series of platinum-ethidium complexes, including the cis and trans isomers of $[Pt(NH_3)_2(Etd)Cl]^{2+}$, *cis*-$[Pt(NH_3)(Etd)Cl_2]^{+}$, and $[Pt(NH_3)_3(Etd)]^{3+}$. Linkage isomers have been identified and the solution thermochromism of the acetate salts

* Abstract published in *Advance ACS Abstracts*, October 15, 1993.

(1) Loehrer, P. J.; Einhorn, L. H. *Ann. Intern. Med.* **1984**, *100*, 704.
(2) Sundquist, W. I.; Lippard, S. J. *Coord. Chem. Rev.* **1990**, *100*, 293.
(3) Tullius, T. D.; Lippard, S. J. *Proc. Natl. Acad. Sci. U.S.A.* **1982**, *79*, 3489.
(4) Merkel, C. M.; Lippard, S. J. *Cold Spring Harbor Symp. Quant. Biol.* **1983**, *47*, 355.
(5) Malinge, J.-M.; Leng, M. *Proc. Natl. Acad. Sci. U.S.A.* **1986**, *83*, 6317.
(6) Malinge, J.-M.; Schwartz, A.; Leng, M. *Nucl. Acids Res.* **1987**, *15*, 1779.
(7) Sundquist, W. I.; Bancroft, D. P.; Chassot, L.; Lippard, S. J. *J. Am. Chem. Soc.* **1988**, *110*, 8559.
(8) Malinge, J.-M.; Sip, M.; Blacker, A. J.; Lehn, J.-M.; Leng, M. *Nucl. Acids Res.* **1990**, *18*, 3887.
(9) Day, J. H. *Chem. Rev.* **1963**, *63*, 65.
(10) Bloomquist, D. R.; Willett, R. D. *Coord. Chem. Rev.* **1982**, *47*, 125.

0002-7863/93/1515-11341$04.00/0

has been investigated. Solutions of the complexes also exhibit pH-dependent color changes when coordinated to duplex DNA, a property which has been exploited to yield structural information about the *cis*-DDP/Etd/DNA ternary complex. Finally, we describe the results of molecular orbital analyses which allow the assignment of the optical transitions responsible for the thermochromism.

Experimental Section

Reagents. Ethidium bromide was purchased from Sigma Chemical Co. and used without further purification. Ethidium nitrate was obtained by reaction of the bromide salt with $AgNO_3$. Dimethylformamide (DMF) was vacuum distilled from BaO and stored over molecular sieves prior to use. All other solvents were of reagent grade or better. *cis*- and *trans*-DDP,[11,12] $(Ph_4P)[Pt(NH_3)Cl_3]$,[13] and $[Pt(NH_3)_3Cl](NO_3)$[14] were prepared according to published procedures.

Instrumentation and Analytical Methods. Unless stated otherwise, a Varian VXR500 NMR spectrometer (500 MHz) was used to record one- and two-dimensional correlated (COSY) ^1H NMR spectra for the compounds. ^1H NMR spectra were obtained in CD_3OD, with chemical shifts (δ) referenced to internal tetramethylsilane. The same instrument equipped with a broad band probe was used to measure 107.25-MHz ^{195}Pt NMR spectra. ^{195}Pt chemical shifts were referenced to an external standard of 0.1 M K_2PtCl_4 in 0.1 M DCl/D_2O (−1624 ppm) and are reported relative to H_2PtCl_6 in D_2O (0 ppm). Broad band ^1H decoupling was not used during acquisition of the ^{195}Pt NMR spectra. Platinum analyses were made by flameless atomic absorption spectroscopy on a Varian AA1475 instrument equipped with a GTA95 graphite furnace. Positive ion fast atom bombardment mass spectra (FABMS) were obtained in glycerol/water or 3-nitrobenzyl alcohol matrices.

Separation of Isomeric Platinum–Ethidium Complexes by Reverse-Phase HPLC. Mixtures of platinum–ethidium linkage isomers, prepared as described below, were separated into isomerically pure products by reverse-phase HPLC on a Waters 600E liquid chromatograph equipped with a Waters 484 tunable absorbance detector operating at 450 nm and a Hewlett Packard 3396A integrator. A 2.2 × 25 cm Whatman Partisil ODS-III column run with aqueous ammonium acetate (0.1 M, pH 5.2)/acetonitrile gradients over 30–60 min was used to effect the separations. Solutions of the separated isomers were immediately frozen and lyophilized to dryness after collection from the column. In a typical injection, ~100–150 mg of crude material could be purified.

Synthesis of *cis*-[Pt(NH$_3$)$_2$(Etd)Cl](OAc)$_2$. *cis*-DDP (1.00 g, 3.33 mmol) was dissolved in 30 mL of DMF and allowed to react with $AgNO_3$ (0.566 g, 3.33 mmol) at ambient temperature in the dark with stirring for 24 h. After centrifugation to remove AgCl, the solution was mixed with ethidium nitrate (1.51 g, 4.0 mmol). The mixture was then stirred at ambient temperature in the dark for 72 h. Subsequent removal of DMF in vacuo yielded a red-orange oil containing the crude mixture of *cis*-$[Pt(NH_3)_2(Etd)Cl](NO_3)_2$ linkage isomers. The oil was washed with 50 mL of diethyl ether and triturated with 100 mL of chloroform to solidify the product and remove excess ethidium nitrate. The solid product was isolated by centrifugation, washed with another 100 mL of chloroform followed by 50 mL of diethyl ether, and dried in air. The yield of crude product was 1.97 g (85% based on *cis*-DDP). Separation of *N3* and *N8* linkage isomers from the crude product mixture was achieved by reverse-phase HPLC as outlined above.

Spectroscopic data for *cis*-$[Pt(NH_3)_2(N3\text{-}Etd)Cl](OAc)_2$ (**1a**): ^1H NMR (CD_3OD) δ 8.86 (d, H1, ^3J = 9.16 Hz), 8.75 (d, H10, ^3J = 9.16 Hz), 8.30 (d, H4, ^4J, unresolved), 7.91 (dd, H2, ^3J = 8.97 Hz, ^4J = 1.57 Hz), 7.81 (m, phenyl, unresolved), 7.65 (m, phenyl, H9, unresolved), 6.59 (d, H7, ^4J = 2.42 Hz), 4.75 (q, CH_2, ^3J = 7.26 Hz), 1.90 (s, 6 H, acetate), 1.59 (t, CH_3, ^3J = 7.26 Hz). ^{195}Pt NMR (MeOH) δ −2342. UV–vis spectral data [λ_{max} in nm, (ϵ in M^{-1} cm^{-1})] H_2O, 444 (4710); MeOH, 480 (6700). FABMS (3-nitrobenzyl alcohol, NBA) *M/z*: 578, $[M - H^+]^+$ (matches theoretical isotope distribution); 561, $[M - H^+ - NH_3]^+$; 543, $[M - H^+ - Cl]^+$; 314, $[Etd]^+$.

Spectroscopic data for *cis*-$[Pt(NH_3)_2(N8\text{-}Etd)Cl](OAc)_2$ (**1b**): ^1H NMR (CD_3OD) δ 8.80 (d, H10, ^3J = 9.07 Hz), 8.79 (d, H1, ^3J = 9.77 Hz), 8.10 (dd, H9, ^3J = 9.10 Hz, ^4J = 2.18 Hz), 7.77 (m, phenyl, unresolved), 7.66 (m, phenyl, unresolved), 7.45 (d, H4, ^4J = 1.99 Hz), 7.45 (dd, H2, ^3J = 9.53 Hz, ^4J = 2.04 Hz), 7.32 (d, H7, ^4J = 2.16 Hz), 4.69 (q, CH_2, ^3J = 7.24 Hz), 1.90 (s, 6 H, acetate), 1.59 (t, CH_3, ^3J = 7.20 Hz). ^{195}Pt NMR (MeOH) δ −2356. UV–vis spectral data [λ_{max} in nm, (ϵ in M^{-1} cm^{-1})] H_2O, 456 (7970); MeOH, 492 (7610). FABMS (3-nitrobenzyl alcohol, NBA) *M/z*: 578, $[M - H^+]^+$ (matches theoretical isotope distribution); 561, $[M - H^+ - NH_3]^+$; 543, $[M - H^+ - Cl]^+$; 314, $[Etd]^+$.

Synthesis of *cis*-[Pt(NH$_3$)$_2$(*N3*-Etd)Cl]Cl$_2$ (1c). An excess of ammonium chloride (15 mg, 280 μmol) was added to an aqueous solution of *cis*-$[Pt(NH_3)_2(N3\text{-}Etd)Cl](OAc)_2$ (5 mg; 8.0 μmol in 1.5 mL of H_2O). The solution was immediately frozen and lyophilized to dryness. The solid was washed with 5 mL of ethanol to remove ammonium acetate and excess ammonium chloride and again lyophilized to dryness. Crystalline material was obtained by refrigeration at 4 °C of a methanol solution of *cis*-$[Pt(NH_3)_2(N3\text{-}Etd)Cl]^{2+}$ containing excess ammonium chloride. The *N8* linkage isomer, *cis*-$[Pt(NH_3)_2(N8\text{-}Etd)Cl]Cl_2$ (**1d**), was also crystallized in this manner from an aqueous solution.

Synthesis of *trans*-[Pt(NH$_3$)$_2$(Etd)Cl](OAc)$_2$. Starting from *trans*-DDP (1.00 g, 3.33 mmol), crude *trans*-$[Pt(NH_3)_2(Etd)Cl](NO_3)_2$ was obtained by the procedure identical to that used for the *cis* compound. Yield: 1.57 g (67% based on *trans*-DDP). The *N3* and *N8* linkage isomers were separated with acetate as the counterion by reverse phase HPLC.

Spectroscopic data for *trans*-$[Pt(NH_3)_2(N3\text{-}Etd)Cl](OAc)_2$ (**2a**): ^1H NMR (measured on a Varian XL300, 300 MHz, CD_3OD) δ 8.89 (d, H1, ^3J = 9.13 Hz), 8.74 (d, H10, ^3J = 9.13 Hz), 8.39 (d, H4, ^4J = 1.82 Hz), 7.93 (dd, H2, ^3J = 8.70 Hz, ^4J = 1.81 Hz), 7.80 (phenyl, unresolved), 7.64 (m, phenyl, H9 unresolved), 6.58 (d, H7, ^4J = 2.43 Hz), 4.77 (q, CH_2), 1.92 (s, 6 H, acetate), 1.53 (t, CH_3). ^{195}Pt NMR spectrum (MeOH) δ −2360. UV–vis spectral data [λ_{max} in nm, (ϵ in M^{-1} cm^{-1})]: H_2O, 456 (4540); MeOH, 524 (4790). FABMS (glycerol/water) *M/z*: 578, $[M - H^+]^+$ (matches theoretical isotope distribution); 561, $[M - H^+ - NH_3]^+$; 543, $[M - H^+ - Cl]^+$; 314, $[Etd]^+$.

Spectroscopic data for *trans*-$[Pt(NH_3)_2(N8\text{-}Etd)Cl](OAc)_2$ (**2b**): ^1H NMR (CD_3OD) δ 8.88 (d, H10, ^3J = 9.28 Hz), 8.81 (d, H1, ^3J = 9.77 Hz), 8.16 (dd, H9, ^3J = 9.03 Hz, ^4J = 2.20 Hz), 7.81 (m, phenyl, unresolved), 7.65 (dd, phenyl, ^3J = 8.06 Hz, ^4J = 1.22 Hz), 7.46 (s, H4), 7.46 (dd, H2, unresolved), 7.23 (d, H7, ^4J = 1.95 Hz), 4.68 (q, CH_2, ^3J = 7.20 Hz), 1.90 (s, 6 H, acetate), 1.54 (t, CH_3, ^3J = 7.08 Hz). ^{195}Pt NMR (MeOH) δ −2377. UV–vis spectral data [λ_{max} in nm, (ϵ in M^{-1} cm^{-1})]: H_2O, 454 (5850); MeOH, 491 (7390). FABMS (glycerol/water) *M/z*: 578, $[M - H^+]^+$ (matches theoretical isotope distribution); 561, $[M - H^+ - NH_3]^+$; 543, $[M - H^+ - Cl]^+$; 314, $[Etd]^+$.

Synthesis of *cis*-[Pt(NH$_3$)(Etd)Cl$_2$](OAc). $(Ph_4P)[Pt(NH_3)Cl_3]$ (1.50 g, 2.28 mmol) was allowed to react with $AgNO_3$ (0.39 g, 2.3 mmol) in 30 mL of DMF at room temperature for 24 h. After centrifugation to remove AgCl, the solution was added to ethidium nitrate (0.95 g, 2.3 mmol). The mixture was then gently stirred at room temperature for 72 h. Subsequent removal of the solvent in vacuo yielded a red-orange oil. The oily product mixture was washed with diethyl ether (25 mL) and triturated with chloroform (50 mL) to solidify the product and remove excess ethidium nitrate. The solidified crude product mixture, which contained insoluble $(Ph_4P)NO_3$, was collected by centrifugation and washed with chloroform and diethyl ether and then air dried. The yield was 1.94 g (77% based on $(Ph_4P)[Pt(NH_3)Cl_3]$, and assuming that the crude product was a 1:1 mixture of the desired Pt complex and $(Ph_4P)NO_3$). Separation of the isomers was achieved through reverse-phase HPLC as described above.

Spectroscopic data for *cis*-$[Pt(NH_3)(N3\text{-}Etd)Cl_2](OAc)$ (**3a**): ^1H NMR (CD_3OD) δ 8.88 (d, H1, ^3J = 8.79 Hz), 8.73 (d, H10, ^3J = 9.28 Hz), 8.35 (d, H4, ^4J = 1.46 Hz), 7.94 (dd, H2, ^3J = 8.79 Hz, ^4J = 1.46 Hz), 7.79 (m, phenyl, unresolved), 7.64 (m, phenyl, H9, unresolved), 6.59 (d, H7, ^4J = 2.44 Hz), 4.77 (q, CH_2, ^3J = 7.08 Hz), 1.92 (s, 3 H, acetate), 1.59 (t, CH_3, ^3J = 7.08 Hz). ^{195}Pt NMR (MeOH) δ -2093. UV–vis spectral data [λ_{max} in nm, (ϵ in M^{-1} cm^{-1})]: H_2O, 449 (8300); MeOH, 486 (8300). FABMS (glycerol/water) *M/z*: 596, $[M]^+$ (matches theoretical isotope distribution); 314, $[Etd]^+$.

Spectroscopic data for *cis*-$[Pt(NH_3)(N8\text{-}Etd)Cl_2](OAc)$ (**3b**): ^1H NMR (CD_3OD) δ 8.80 (2d, H1, H10, unresolved), 8.11 (dd, H9, ^3J = 9.03 Hz, ^4J = 2.20 Hz), 7.78 (m, phenyl, unresolved), 7.66 (m, phenyl, unresolved), 7.46 (m, H2, H4, unresolved), 7.28 (d, H7, ^4J = 1.95 Hz), 4.69 (q, CH_2, ^3J = 7.45 Hz), 1.93 (s, 3 H, acetate), 1.54 (t, CH_3, ^3J = 7.45 Hz). ^{195}Pt NMR (MeOH) δ −2109. UV–vis spectral data [λ_{max} in nm, (ϵ in M^{-1} cm^{-1})]: H_2O, 452 (8720); MeOH, 486 (7310). FABMS (glycerol/water) *M/z*: 596, $[M]^+$ (matches theoretical isotope distribution); 314, $[Etd]^+$.

Synthesis of [Pt(NH$_3$)$_3$(Etd)](OAc)$_3$. $[Pt(NH_3)_3Cl]Cl$ (0.634 g, 2.0 mmol) was allowed to react with $AgNO_3$ (0.700 g, 4.1 mmol) in DMF

(11) Dhara, S. C. *Indian J. Chem.* **1970**, *8*, 193.
(12) Kaufman, G. B.; Cowan, D. O. *Inorg. Synth.* **1963**, *7*, 239.
(13) Abrams, M. J.; Giandomenico, C. M.; Vollano, J. F.; Schwartz, D. A. *Inorg. Chim. Acta* **1987**, *131*, 3.
(14) Lepre, C. A. Ph.D. Thesis, Massachusetts Institute of Technology, 1989.

at room temperature for 24 h. The mixture was centrifuged to remove precipitated AgCl and ethidium nitrate (0.83 g, 2.2 mmol) was added. The solution was stirred for 72 h, evaporated to dryness in vacuo, and washed with diethyl ether. A red-orange solid containing a mixture of *N3* and *N8* linkage isomers was isolated after trituration with chloroform. The yield was 1.47 g (98% based on $[Pt(NH_3)_3Cl]Cl$). The *N3* and *N8* isomers were separated with acetate as counterion by reverse-phase HPLC. Alternatively, $[Pt(NH_3)_3Cl](NO_3)$ was used as starting material.

Spectroscopic data for $[Pt(NH_3)_3(N3\text{-Etd})](OAc)_3$ (**4a**): ^1H NMR (CD_3OD) δ 8.56 (d, H1, ^3J = 9.28 Hz), 8.53 (d, H10, ^3J = 9.28 Hz), 7.82 (s, H4), 7.76 (m, phenyl, unresolved), 7.68 (d, H2, ^3J = 8.79 Hz), 7.59 (m, phenyl, unresolved), 7.52 (dd, H9, ^3J = 9.03 Hz, ^4J = 2.20 Hz), 6.41 (d, H7, ^4J = 1.95 Hz), 4.64 (q, CH_2, ^3J = 7.08 Hz), 1.90 (s, 9 H, acetate), 1.51 (t, CH_3, ^3J = 7.08 Hz). ^{195}Pt NMR (MeOH) δ -2532. UV–vis spectral data [λ_{max} in nm, (ϵ in M^{-1} cm^{-1})]: H_2O, 443 (4370); MeOH, 632 (11860). FABMS (glycerol/water) *M/z*: 558, $[M - 2H^+]^+$ (matches theoretical isotope distribution); 524, $[M - 2H^+ - 2NH_3]^+$; 507, $[M - 2H^+ - 3NH_3]^+$; 314, $[Etd]^+$.

Spectroscopic data for $[Pt(NH_3)_3(N8\text{-Etd})](OAc)_3$ (**4b**): ^1H NMR (CD_3OD) δ 8.82 (d, H10, ^3J = 9.28 Hz), 8.78 (d, H1, ^3J = 9.77 Hz), 8.16 (dd, H9, ^3J = 9.03 Hz, ^4J = 2.20 Hz), 7.81 (m, phenyl, unresolved), 7.63 (m, phenyl, unresolved), 7.46 (dd, H2, unresolved), 7.45 (s, H4), 7.23 (d, H7, ^4J = 2.44 Hz), 4.67 (q, CH_2, ^3J = 7.08 Hz), 1.87 (s, 9 H, acetate), 1.53 (t, CH_3, ^3J = 7.08 Hz). ^{195}Pt NMR (MeOH) δ -2563. UV–vis spectral data [λ_{max} in nm, (ϵ in M^{-1} cm^{-1})]: H_2O, 454 (5900); MeOH, 490 (3970). FABMS (glycerol/water) *M/z*: 558, $[M - 2H^+]^+$ (matches theoretical isotope distribution); 524, $[M - 2H^+ - 2NH_3]^+$; 507, $[M - 2H^+ - 3NH_3]^+$; 314, $[Etd]^+$.

Visible Absorption Spectra and DNA Binding of Platinum–Ethidium Complexes. Spectra were obtained on a Perkin-Elmer Lambda 7 spectrophotometer equipped with a data station unless otherwise specified. Extinction coefficients were obtained using solutions in which the platinum concentration was determined by atomic absorption spectroscopy. Spectra for pH-dependent studies were obtained by titrating aqueous solutions of the complexes with 0.1 N NaOH and monitoring the visible absorption spectrum at various pH values. An Orion Research Model 231 pH meter equipped with a semimicro Ross combination pH electrode was used to measure the solution pH in the cell immediately before acquisition of each spectrum. Standardized buffer solutions were used to calibrate the pH meter prior to each titration. For pH-dependent spectra of ternary complexes generated from the reactions of **1a** and **1b** with DNA, 1 mL of a 2.5 mM solution of calf thymus DNA was used. The complexes were added from freshly prepared stock solutions at a formal Pt:nucleotide ratio (r_f) of 0.1. The platinum complexes were allowed to react with the DNA at 4 °C in the dark for 12 h. Formation of the ternary complex from the promoted reaction of *cis*-DDP with DNA in the presence of ethidium bromide was carried out as described.[5] Samples of the DNA bound isomers and the ternary complex were then titrated with 0.1 N NaOH as described above.

Compounds *cis*-$[Pt(NH_3)_2(N3\text{-Etd})Cl](OAc)_2$ (**1a**), *trans*-$[Pt(NH_3)_2(N3\text{- or }N8\text{-Etd})Cl](OAc)_2$ (**2a,b**), and $[Pt(NH_3)_3(N3\text{ or }N8\text{-Etd})](OAc)_3$ (**4a,b**) were subjected to temperature-dependent spectroscopic analysis in a Hewlett Packard 8452A diode-array spectrophotometer. A sealed quartz cell (Hellma 220-QS) placed in a cryostat (low-temperature Specac IR cell modified for UV–vis spectroscopy) was used as the sample container. An anhydrous methanol solution of the complex was sealed and mounted in the apparatus under an inert atmosphere. Spectra were recorded in the temperature range 223–323 K at *ca.* 5 K increments for most of the compounds, and from 203 to 293 K for $[Pt(NH_3)_3(N3\text{-Etd})](OAc)_3$. The temperature in the cell was monitored by using a Cole-Parmer thermocouple. All samples were purified twice by HPLC prior to use. The quality and stoichiometry of the samples were checked by ^1H NMR spectroscopy with an appropriate delay time ($>5T_1$).

X-ray Crystallography. ***cis*-$[Pt(NH_3)_2(N3\text{-Etd})Cl]Cl_2\cdot 2.5H_2O$.** A dark orange-red crystal of dimensions 0.05 × 0.175 × 0.225 mm was mounted on the end of a glass fiber with silicone grease. All measurements were made at −100 °C. Open counter ω-scans on several low angle reflections revealed the crystal quality to be marginal, with peak widths at half height of 0.5°. Unit cell parameters were obtained from a least squares fit of 25 centered reflections. Periodic monitoring of three standard reflections throughout the data collection showed severe decay (40%) which limited the useful reflections to a relatively low angle range, $2\theta <$ 35°. A decay correction was applied to account for the loss of intensity. Space group $P\bar{1}$ was chosen on the basis of the Wilson plot statistics and confirmed by the successful refinement of the structure. Data were reduced and the structure solved following procedures commonly used in our laboratory.[15] Absorption was taken into account by use of the program DIFABS.[16] The lattice contained a region of partially occupied and/or disordered solvent which was included in the refinement as five partially occupied H_2O molecules; the presence of additional disordered solvent is not ruled out. Other information is provided in Table I and as supplementary material (Tables S1–S6).

Table I. Experimental Details of the X-ray Diffraction Studies of **1c** and **1d**

	1c·2.5H_2O	**1d**·2H_2O
formula	$PtC_{21}H_{27}O_{2.5}N_5Cl_3$	$PtC_{21}H_{26}O_2N_5Cl_3$
fw	690.92	681.92
cryst syst	triclinic	triclinic
space group	$P\bar{1}$	$P\bar{1}$
a, Å	7.939(2)	11.547(2)
b, Å	12.919(4)	12.906(3)
c, Å	14.886(6)	9.384(2)
α, deg	113.69(3)	105.92(2)
β, deg	94.66(3)	93.69(1)
γ, deg	90.21(3)	74.84(2)
Z	2	2
V, Å^3	1392.5(8)	1292.9(4)
d_{calcd}, g/cm^3	1.640	1.744
T, K	173	173
no. of reflctns collctd	1768	4554
data collctn range, deg	$4 \le 2\theta \le 35$	$3 \le 2\theta \le 50$
data limits	$+h,\pm k,\pm l$	$+h,\pm k,\pm l$
no. of unique data[a]	1459	3380
no. of parameters	182	301
μ(Mo Kα), cm^{-1}	54.02	57.96
transmission coeff	0.76–1.24[d]	0.74–1.00
R[b]	0.063	0.052
R_w[c]	0.076	0.070
largest shift/esd, final	0.01	0.06
largest peak, e/Å^3	1.35[e]	2.47[e]

[a] $I > 3\sigma(I)$. [b] $R = \sum||F_o|-|F_c||/\sum|F_o|$. [c] $R_w = [\sum w(|F_o|-|F_c|)^2/\sum w|F_o|^2]^{1/2}$, where $w = 1/\sigma^2(F)$ and $\sigma^2(F)$ is defined in ref 15. [d] From DIFABS. [e] Near Cl^- counterion.

***cis*-$[Pt(NH_3)_2(N8\text{-Etd})Cl]Cl_2\cdot 2H_2O$.** An orange crystal of dimensions 0.075 × 0.167 × 0.225 mm was mounted on a glass fiber with epoxy cement. The crystal quality was good as judged by open counter ω-scans on several strong, low-angle reflections which revealed an average width at half height of 0.27°. Unit cell parameters were obtained by a least-squares fit of 25 well-centered reflections, and space group $P\bar{1}$ was chosen and confirmed by successful refinement of the structure. The crystal did not decay appreciably (<6%) during the course of data collection. Two lattice water molecules, disordered over four independent positions, were successfully located and refined. Additional information may be found in Table I and in the supplementary material (Tables S7–12).

Computational Procedures. Global Analysis. UV–visible absorption spectra recorded over a wide temperature range were analyzed with a locally developed global analysis program[17,18] written in the Labview2 environment (National Instruments) for a Macintosh IIfx computer (Apple Co.). Two intensity vectors corresponding to the spectra of the individual orange and blue species in equilibrium with one another, as well as the thermodynamic parameters $\Delta H°$ and $\Delta S°$, were optimized iteratively by means of a nonlinear least-squares procedure. In this manner, $2n + 2$ (or $2n + 3$, vide infra) parameters, where n is the number of wavelengths (typically 100) at which an absorbance reading was made, were fit to the experimental data. Initial values for $\Delta H°$ and $\Delta S°$ were obtained from single wavelength analyses, usually chosen in the vicinity of the absorption maxima where the optical density changes greatly exceeded the possible experimental errors. These values were then inserted into the multiwavelength fitting program which was initialized with two spectral vectors, corresponding to the lowest (orange) and highest (blue) temperatures. Convergence typically occurred after 5 to 10 iterations, yielding spectra of the individual species as well as the standard free enthalpy and entropy values for the equilibrium under consideration. One of two models employed corresponds to temperature-dependent equilibria that occur for stoichiometric mixtures of the platinum complexes and acetate counterion, details of which are briefly presented in the Results

(15) Carnahan, E. M.; Rardin, R. L.; Bott, S. G.; Lippard, S. J. *Inorg. Chem.* **1992**, *31*, 5193.
(16) Walker, N.; Stuart, D. *Acta Crystallogr.* **1983**, *A39*, 158.
(17) Gampp, H.; Maeder, M.; Meyer, C. J.; Zuberbühler, A. D. *Talanta* **1985**, *32*, 95.
(18) Beechem, J. M.; Ameloot, M.; Brand, L. *Anal. Instrum.* **1985**, *14*, 379.

Table II. Selected ^{195}Pt and ^{1}H NMR Chemical Shift Data for Platinum–Ethidium Complexes[a]

complex	^{195}Pt	H1	H2	H4	H7	H9	H10
ethidium		8.62	7.36	7.37	6.45	7.55	8.56
cis-[Pt(NH$_3$)$_2$(*N3*-Etd)Cl](OAc)$_2$	−2342	8.86 (0.14)	7.91 (0.55)	8.30 (0.93)	6.59 (0.14)	7.65 (0.10)	8.75 (0.19)
cis-[Pt(NH$_3$)$_2$(*N8*-Etd)Cl](OAc)$_2$	−2356	8.79 (0.17)	7.45 (0.09)	7.45 (0.08)	7.32 (0.77)	8.10 (0.55)	8.80 (0.24)
trans-[Pt(NH$_3$)$_2$(*N3*-Etd)Cl](OAc)$_2$	−2360	8.89 (0.27)	7.93 (0.57)	8.39 (1.02)	6.58 (0.13)	7.64 (0.09)	8.74 (0.18)
trans-[Pt(NH$_3$)$_2$(*N8*-Etd)Cl](OAc)$_2$	−2377	8.81 (0.19)	7.46 (0.10)	7.46 (0.09)	7.23 (0.78)	8.16 (0.51)	8.88 (0.32)
cis-[Pt(NH$_3$)(*N3*-Etd)Cl$_2$](OAc)	−2093	8.88 (0.26)	7.94 (0.58)	8.35 (0.98)	6.59 (0.14)	7.64 (0.09)	8.73 (0.17)
cis-[Pt(NH$_3$)(*N8*-Etd)Cl$_2$](OAc)	−2109	8.80 (0.18)	7.46 (0.10)	7.46 (0.09)	7.28 (0.73)	8.11 (0.56)	8.80 (0.24)
[Pt(NH$_3$)$_3$(*N3*-Etd)](OAc)$_3$	−2532	8.56 (−0.06)	7.68 (0.32)	7.82 (0.45)	6.41 (−0.04)	7.52 (−0.03)	8.53 (−0.03)
[Pt(NH$_3$)$_3$(*N8*-Etd)](OAc)$_3$	−2563	8.78 (0.18)	7.46 (0.10)	7.45 (0.08)	7.23 (0.78)	8.16 (0.51)	8.82 (0.26)

[a] Chemical shifts in ppm relative to TMS at 0 ppm. Values in parentheses denote chemical shifts downfield (positive) or upfield (negative) versus free ethidium. The ethidium ring numbering scheme is given in the text.

and Discussion section. The other model takes into account deviations from this stoichiometry, and its formulation is provided as supplementary material.

Molecular Orbital Calculations. Fenske–Hall calculations were performed on a VAXstation 3100 with the program developed by Hall et al.[19] Basis functions were derived from the Xα atomic orbitals of Herman and Skillman[20] with the use of an Xα-to-Slater basis program.[21,22]

Model calculations were made on the following acidic forms of the complexes: (i) *cis*-[Pt(NH$_3$)$_2$(*N3*-Mtd)Cl]$^{2+}$, (ii) *cis*-[Pt(NH$_3$)$_2$(*N8*-Mtd)Cl]$^{2+}$, (iii) *trans*-[Pt(NH$_3$)$_2$(*N8*-Mtd)Cl]$^{2+}$, and (iv) [Pt(NH$_3$)$_3$(*N8*-Mtd)]$^{3+}$, where Mtd is methidium, an ethidium analogue with methyl replacing the ethyl group, as well as their corresponding deprotonated forms. For the former, geometric parameters of the Pt coordination shell were similar to those determined in the X-ray diffraction study of *cis*-[Pt(NH$_3$)$_2$(*N3*-Etd)Cl]Cl$_2$, namely, Pt–N(NH$_3$) = 2.00 Å, Pt–Cl = 2.29 Å, Pt–N(N3 or N8) = 2.06 Å, C–N (coordinated exocyclic amine) = 1.44 Å, C–N (free exocyclic amine) = 1.41 Å, and N–C (the methyl attached to N5) = 1.51 Å. The C–C (C–N) distances within all aromatic rings and the C–H and N–H distances were assumed to be 1.38, 1.08, and 1.00 Å, respectively. The geometry around N3 was chosen so that the dihedral angle between the phenanthridinium ring plane and the Pt coordination plane was 113°, the value observed in the X-ray structure determination. The orientation of the phenyl group of methidium was determined to be approximately perpendicular to the ring plane and preserved in the calculations. For the deprotonated forms, the geometric parameters of the first coordination shell of the Pt center and the orientation of the methidium ring were taken from the X-ray structural analysis of *cis*-[Pt(NH$_3$)$_2$(*N9*-9-aminoacridine)Cl]$^{2+}$ [23] (see Results and Discussion). The geometry used was Pt–N3 (N8) = 1.99 Å, Pt–N (NH$_3$) = 2.04 Å, Pt–Cl = 2.31 Å, N3 (N8)–C = 1.30 Å, and the dihedral angle = 105°. The remaining geometric parameters were the same as those described above for the protonated form. The master coordinate and the coordinate of the Pt center were chosen to be consistent with the convention (Z unique) of square-planar geometry, and the Y axis was always coincident with the Pt–N (exocyclic amine) bond.

Results and Discussion

Synthesis and Purification of Platinum–Ethidium Complexes. A series of platinum(II)–ethidium complexes containing different combinations of ammine and chloride ligands was prepared as outlined in eq 1. For each of the four starting complexes, n =

$$[Pt(NH_3)_nCl_{4-n}]^{(n-2)} + AgNO_3 \xrightarrow[\text{DMF, rt, 16 h}]{-AgCl} \xrightarrow[\text{DMF, rt, 2–3 days}]{Etd(NO_3)} [Pt(NH_3)_n(Etd)Cl_{3-n}](NO_3)_n \quad (1)$$

1, 2 (initial cis or trans stereochemistry yielding cis or trans product, respectively), or 3, the reactions proceeded via the replacement of a single chloride ligand with an ethidium cation. The use of silver nitrate to remove chloride from each platinum precursor complex accelerated the subsequent ethidium substitution reaction. This two-step procedure yielded products of greater stoichiometric and stereochemical purity than could be obtained by direct reaction of the starting platinum chloride complexes with ethidium.[24] The reactions were monitored by ^{195}Pt NMR spectroscopy. Two products, subsequently identified as *N3* and *N8* ethidium linkage isomers, vide infra, invariably formed in approximately equimolar concentrations. Following initial workup to remove excess ethidium and DMF, the isomers were separated and purified by reverse-phase HPLC. A mixed mobile phase of acetonitrile and aqueous ammonium acetate buffer was employed, and the separations were performed under slightly acidic conditions (pH 5.2) in order to minimize diffusion of the products on the HPLC column caused by an acid/base equilibrium which was evident at higher pH. Purified samples were stored as solids at −20 °C. Although degradation of the *N8* isomers is very slow in solution, the *N3* isomers inevitably decompose in both aqueous and alcoholic solvents. The most unstable complex, *trans*-[Pt(NH$_3$)$_2$(*N3*-Etd)Cl](OAc)$_2$, was observed by ^{1}H and ^{195}Pt NMR spectroscopy and HPLC to lose ethidium and subsequently rearrange to the corresponding *N8* isomer.

NMR Spectroscopic Characterization of Platinum–Ethidium Complexes. Following purification, each platinum–ethidium complex was analyzed spectroscopically. The composition of ligands in the coordination sphere was established by ^{195}Pt NMR spectroscopy, taking advantage of the diagnostic ^{195}Pt chemical shifts, PtN_4 ~ −2550 ppm, PtN_3Cl ~ −2350 ppm, and PtN_2Cl_2 ~ −2100 ppm (Table II). FAB mass spectral analyses were also performed on all complexes, providing further confirmation of the structural formulas assigned by the ^{195}Pt NMR spectra. These analyses did not, however, allow unambiguous assignment of N3 and N8 linkage isomers, and the site of platinum coordination was therefore determined by ^{1}H NMR spectroscopy as outlined below.

The phenanthridium ring of Etd consists of two distinct spin systems (H1, H2, H4 and H7, H9, H10), which have been fully assigned for the free ligand (Table II).[25–28] The two spin systems are readily differentiated since the H7 proton (d, 6.45 ppm, ^{4}J = 2.38 Hz) is shielded by the adjacent phenyl ring and therefore resonates at significantly higher field than any other aromatic proton in the cation. The H7 proton was assigned in a similar manner for the platinum–ethidium complexes, and the remaining phenanthridium proton assignments were determined on the basis of 1D and 2D COSY experiments. Full assignments are given in Table II.

(19) Hall, M. B.; Fenske, R. F. *Inorg. Chem.* **1972**, *11*, 768.
(20) Herman, F.; Skillman, S. *Atomic Structure Calculations*; Prentice-Hall: Englewood Cliffs, NJ, 1963.
(21) Bursten, B. E.; Fenske, R. F. *J. Chem. Phys.* **1977**, *67*, 3138.
(22) Bursten, B. E.; Jensen, J. R.; Fenske, R. F. *J. Chem. Phys.* **1978**, *68*, 3320.
(23) Sundquist, W. I.; Bancroft, D. P.; Lippard, S. J. *J. Am. Chem. Soc.* **1990**, *112*, 1590.
(24) Hollis, L. S.; Amundsen, A. R.; Stein, E. W. *J. Med. Chem.* **1989**, *32*, 128.
(25) Kreishman, G. P.; Chan, S. I.; Bauer, W. *J. Mol. Biol.* **1971**, *61*, 45.
(26) Thomas, G.; Roques, B. *FEBS Lett.* **1972**, *26*, 169.
(27) Krugh, T. R.; Reinhardt, C. G. *J. Mol. Biol.* **1975**, *97*, 133.
(28) Firth, W. J.; Watkins, C. L.; Graves, D. E.; Yielding, L. W. *J. Heterocycl. Chem.* **1983**, *20*, 759.

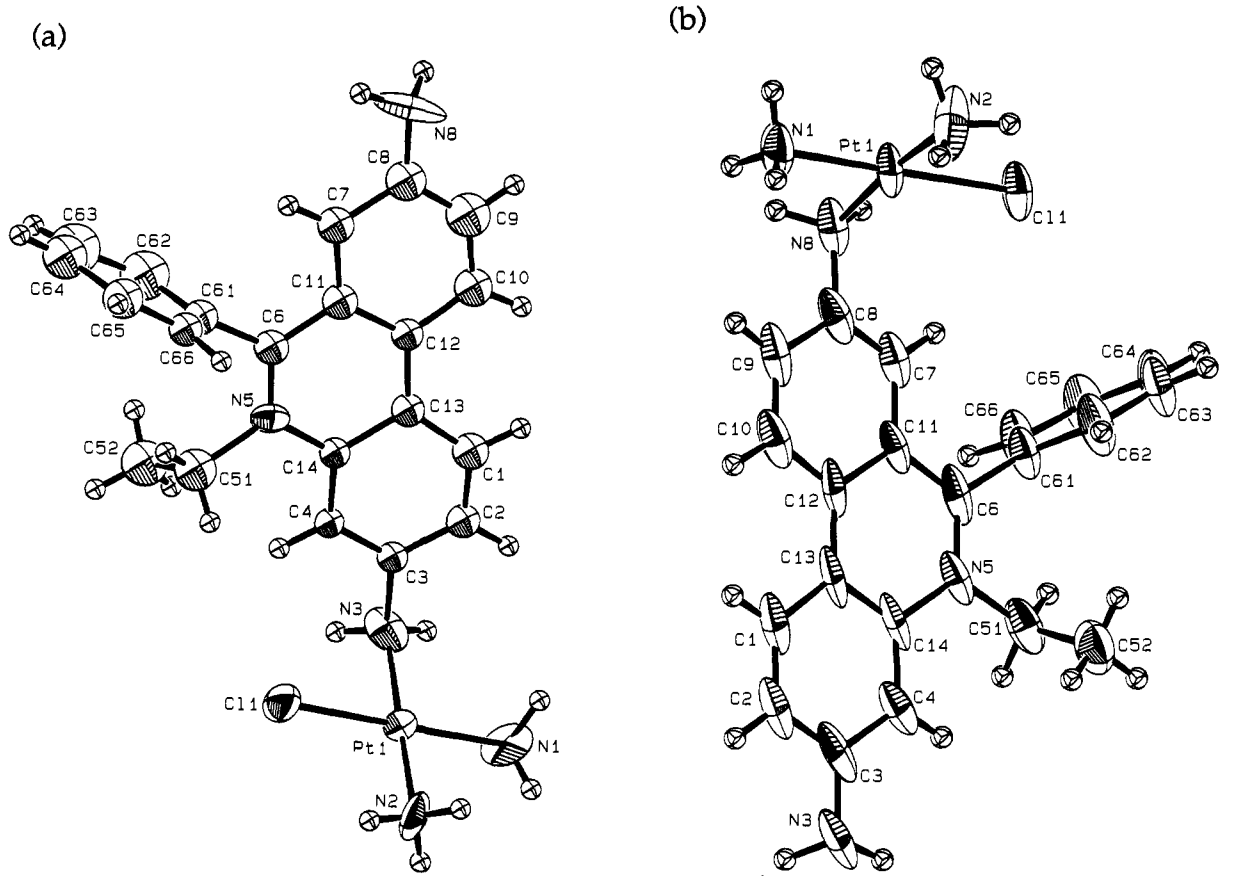

Figure 1. Structures of *cis*-$[Pt(NH_3)_2(N3\text{-Etd})Cl]^{2+}$ (a) and *cis*-$[Pt(NH_3)_2(N8\text{-Etd})Cl]^{2+}$ (b) cations showing the 50% probability ellipsoids and atom labeling schemes.

The site of platinum binding was revealed by the characteristic paramagnetic deshielding of adjacent protons, H2 and H4 in the *N3* isomers and H7 and H9 in the *N8* isomers.[29,30] As evident from Table II, this downfield shift is most pronounced at the H4 and H7 positions. For *N3* isomers of both PtN_3Cl and PtN_2Cl_2 cores, the H4 proton resonances were shifted downfield by more than 0.9 ppm versus free ethidium whereas the distal H7 protons were shifted by less than 0.2 ppm. Conversely, in the corresponding *N8* isomers, the H7 resonances were shifted downfield by more than 0.7 ppm whereas the H4 resonances are not significantly shifted (<0.1 ppm). It is noteworthy that the downfield shift of the H4 resonance in $[Pt(NH_3)_3(N3\text{-Etd})](OAc)_3$ (**4a**), 0.45 ppm, is much smaller than that of the other *N3* isomers. This result reflects the fact that all the Pt–Etd complexes exist as a mixture of protonated and deprotonated forms (vide infra). Paramagnetic deshielding in the latter is much smaller owing to lower formal charge. The observed chemical shifts in the ^1H NMR spectra are the average values of the two forms in the limit of fast proton exchange. Although most of the Pt–Etd complexes have comparable or lower acidity than acetic acid in methanol solution, the cation in $[Pt(NH_3)_3(N3\text{-Etd})](OAc)_3$ is much more acidic and hence exists predominantly in its deprotonated form. Consequently, a significant reduction in the paramagnetic deshielding occurs for this trication. The greater acidity of the *N3* isomers in general, a phenomenon discussed in more detail below, similarly influences the ^{195}Pt chemical shifts, which systematically appear at slightly higher fields than for the corresponding *N8* isomers (Table II).

Structural Characterization of *cis*-$[Pt(NH_3)_2(N3\text{-Etd})Cl]Cl_2\cdot 2.5H_2O$ and *cis*-$[Pt(NH_3)_2(N8\text{-Etd})Cl]Cl_2\cdot 2H_2O$. In order to confirm and extend the information afforded by the spectroscopic analyses of the platinum–ethidium complexes, we carried out X-ray crystal structure determinations of an *N3* isomer, *cis*-$[Pt(NH_3)_2(N3\text{-Etd})Cl]Cl_2\cdot 2.5H_2O$ (**1c**), and an *N8* isomer, *cis*-$[Pt(NH_3)_2(N8\text{-Etd})Cl]Cl_2\cdot 2H_2O$ (**1d**). These complexes formed single crystals suitable for X-ray diffraction studies following slow cooling of either methanolic (**1c**) or aqueous (**1d**) solutions containing nearly saturating concentrations of ammonium chloride, added to inhibit hydrolysis of the Pt–Cl bond during crystallization. The data obtained for *cis*-$[Pt(NH_3)_2(N3\text{-Etd})Cl]Cl_2\cdot 2.5H_2O$ are of poor quality, owing to significant loss of scattering intensity during data collection, but are sufficient to provide a definitive assessment of linkage isomer and other geometric parameters. ORTEP diagrams showing structures of the *cis*-$[Pt(NH_3)_2(N3\text{-Etd})Cl]^{2+}$ and *cis*-$[Pt(NH_3)_2(N8\text{-Etd})Cl]^{2+}$ cations are presented in Figure 1, and a selection of interatomic distances and angles is given in Table III.

As anticipated, the structures confirm the spectroscopic assignment of *N3* and *N8* linkage isomers. The platinum coordination geometry is square planar in both complexes with normal Pt–Cl and Pt–NH_3 bond lengths (Table III). Several lines of evidence indicate that the coordinated amino groups are protonated in both complexes. Both *N8* protons were located from difference Fourier maps in the structure of *cis*-$[Pt(NH_3)_2(N8\text{-Etd})Cl]Cl_2\cdot 2H_2O$. The N3(8)–C3(8) bond length, 1.44 Å, is significantly longer than the N9–C9 bond length (1.32 Å) found in *cis*-$[Pt(NH_3)_2(N9\text{-9-AA})Cl]^+$,[23] where the coordinated 9-amino group is deprotonated and the N9–C9 linkage has imino bond (N=C) character. Moreover, both **1c** and **1d** have Pt–NH_2–C bond angles characteristic of sp^3-hybridized nitrogen atoms (Table III). Other aspects of the Etd coordination and ring geometry are similar to those reported previously.[31-33]

The ethyl group is rotated out of the phenanthridium plane in

(29) Buckingham, A. D.; Stevens, P. J. *J. Chem. Soc.* **1964**, 2747.
(30) Miller, R. G.; Stauffer, R. D.; Fahey, D. R.; Parnell, D. R. *J. Am. Chem. Soc.* **1970**, *92*, 1511.
(31) Davies, G. R.; Hewertson, W.; Mais, R. H. B.; Owston, P. G. *J. Chem. Soc., Chem. Commun.* **1967**, 423.
(32) Subramanian, E.; Trotter, J.; Bugg, C. E. *J. Cryst. Mol. Struct.* **1971**, *1*, 3.

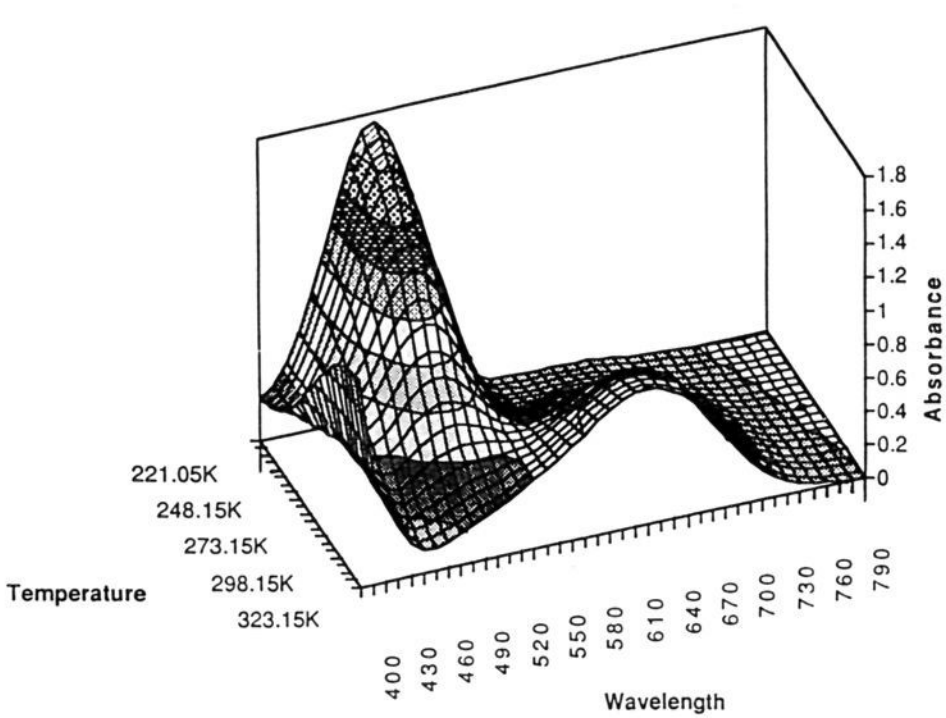

Figure 2. Temperature dependence of the optical spectrum of $[Pt(NH_3)_3(N8\text{-Etd})](OAc)_3$ (**4b**) in MeOH between −50 and 50 °C. Spectra were taken at 5° increments.

Table III. Selected Bond Lengths (Å) and Angles (deg) in *cis*-$[Pt(NH_3)_2(N3\text{-Etd})Cl]Cl_2\cdot 2.5H_2O$ (**1c**) and *cis*-$[Pt(NH_3)_2(N8\text{-Etd})Cl]Cl_2\cdot 2H_2O$ (**1d**)[a]

	1c	1d		1c	1d
		Distances			
Pt–Cl	2.282(7)	2.291(3)	C3–C4	1.36(3)	1.41(2)
Pt–N1	2.03(2)	2.06(1)	C4–C14	1.36(3)	1.39(2)
Pt–N2	1.99(2)	2.01(1)	C6–C11	1.41(3)	1.43(2)
Pt–N3	2.05(2)		C7–C11	1.42(3)	1.43(2)
Pt–N8		2.08(1)	C7–C8	1.43(3)	1.36(2)
N3–C3	1.45(3)	1.38(2)	C8–C9	1.33(3)	1.39(2)
N8–C8	1.38(3)	1.43(2)	C9–C10	1.34(3)	1.37(2)
N5–C6	1.32(3)	1.33(2)	C10–C12	1.39(3)	1.41(2)
N5–C51	1.57(3)	1.49(2)	C12–C13	1.40(3)	1.44(2)
N5–C14	1.40(3)	1.41(1)	C11–C12	1.39(3)	1.41(1)
C1–C2	1.33(3)	1.37(2)	C13–C14	1.45(3)	1.40(2)
C1–C13	1.38(3)	1.40(1)	C51–C52	1.52(4)	1.52(2)
C2–C3	1.35(3)	1.39(2)			
		Angles			
Cl–Pt–N1	178.4(8)	178.6(3)	C14–C13–C1	114(2)	117(1)
Cl–Pt–N2	88.1(6)	88.7(3)	C14–C13–C12	118(2)	119(1)
Cl–Pt–N3	91.4(6)		C14–N5–C6	123(2)	122(1)
Cl–Pt–N8		88.3(3)	N5–C6–C11	121(2)	121(1)
N1–Pt–N2	91.4(9)	90.0(5)	C6–C11–C12	119(2)	119(1)
N1–Pt–N3	89.0(9)		C11–C12–C13	121(2)	119(1)
N1–Pt–N8		93.1(4)	C11–C7–C8	117(2)	119(1)
N2–Pt–N3	178.2(9)		C7–C8–C9	116(2)	122(1)
N2–Pt–N8		174.5(5)	C7–C8–N8	122(2)	120(1)
Pt–N3–C3	113(1)		C8–C9–C10	128(3)	120(1)
Pt–N8–C8		112.5(7)	C9–C8–N8	122(3)	118(1)
C1–C2–C3	122(2)	120(1)	C2–C3–N3	120(2)	119(1)
C2–C3–C4	118(2)	119(1)	C4–C3–N3	122(2)	122(1)
C3–C4–C14	122(2)	119(1)	C9–C10–C12	120(2)	121(1)
C4–C14–C13	120(2)	122(1)	N5–C51–C52	110(2)	110(1)

[a] See Figure 1 for atom labeling scheme. Numbers in parentheses are estimated standard deviations.

both complexes, the C6–N5–C51–C52 torsion angles being 95(3)° in *cis*-$[Pt(NH_3)_2(N3\text{-Etd})Cl]Cl_2\cdot 2.5H_2O$ and 97(1)° in *cis*-$[Pt(NH_3)_2(N8\text{-Etd})Cl]Cl_2\cdot 2H_2O$. The relative orientations of the platinum coordination plane and ethyl group differ in the two complexes, however, presumably as a result of their somewhat disparate crystal packing environments. Specifically, *cis*-$[Pt(NH_3)_2(N8\text{-Etd})Cl]Cl_2\cdot 2H_2O$ crystallizes with the platinum coordination plane and ethyl group projecting from the same side of the phenanthridium ring plane, whereas *cis*-$[Pt(NH_3)_2(N3\text{-Etd})Cl]Cl_2\cdot 2.5H_2O$ crystallizes with the two moieties projecting from opposite sides of the plane (Figure 1). Such conformational isomers should interconvert in solution, however, requiring only rotation about the Pt–NH_2–C single bond. The phenanthridium rings stack in a head-to-tail manner across an inversion center in both complexes, with interplanar distances of ~3.4 Å.

The crystal lattices for **1c** and **1d** contain two chloride ions and several solvent molecules in addition to the cationic platinum moieties. One of the chloride ions in **1d** is disordered over two positions with one of the sites being near the inversion center at (1/2, 0, 0). Both **1c** and **1d** contain regions of disordered solvent in the crystal lattice. In the case of **1c**, it was not possible to discern from the Fourier maps whether the solvent was H_2O or MeOH because of the poor quality of the data set. The final refined model contained 2.5 H_2O molecules/platinum species. Similar solvent disorder in **1d** was modeled as 2.0 H_2O molecules/platinum complex.

Electronic Spectra and Solution Thermochromism of Platinum–Ethidium Acetate Complexes. In aqueous solution, all Pt–Etd complexes have an absorption band at 450 nm (22 000 cm^{-1}), which is blue-shifted from that of free ethidium (λ_{max} 481 nm, 20 800 cm^{-1}).[34] In MeOH solution the band shifts to lower energy by ca. 1800 cm^{-1} (0.22 eV) for all the complexes, behavior characteristic of chromophores exhibiting an $n \rightarrow \pi^*$ transition.[35] A similar bathochromic shift occurs for ethidium bromide.

Solutions of the platinum–ethidium acetate compounds display remarkable thermochromism in polar solvents (the compounds are insoluble in nonpolar solvents). Initially, we observed that a solution of *cis*-$[Pt(NH_3)_2(N3\text{-Etd})Cl](OAc)_2$ in methanol changed color from orange to deep blue upon warming from −20 to 50 °C. In order to study this phenomenon in detail, visible absorption spectra of the platinum–ethidium complexes were recorded as a function of temperature in methanol. Figure 2

(33) Courseille, P. C.; Busetta, B.; Hospital, M. *Acta Crystallogr.* **1974**, *B30*, 2631.

(34) Zimmermann, I.; Zimmermann, H. W. *Ber. Bunsen-Ges. Phys. Chem.* **1977**, *81*, 81.

(35) Drago, R. S. *Physical Methods for Chemists*; Saunders College Publishing: Ft. Worth, 1992.

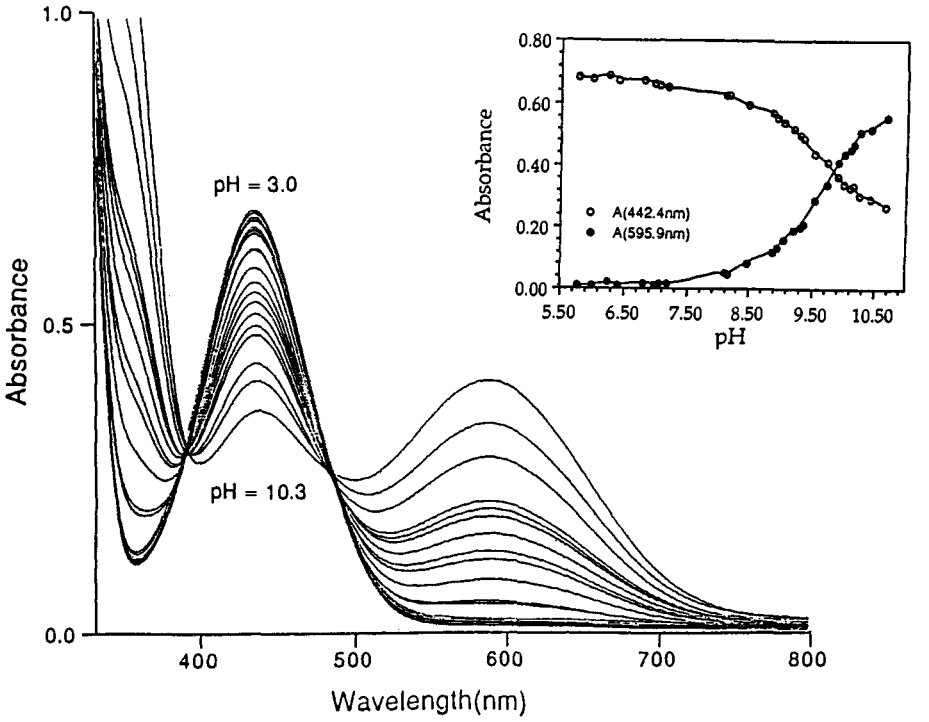

Figure 3. Optical absorption spectra of *cis*-[Pt(NH$_3$)$_2$(*N3*-Etd)Cl](OAc)$_2$ (**1a**) in aqueous solution as a function of pH. The inset plots the pH dependence of the absorption near the absorption maxima.

displays the UV–vis absorption spectra recorded between −50 and 50 °C at 5° increments of a methanolic solution of [Pt(NH$_3$)$_3$(*N8*-Etd)](OAc)$_3$. The thermochromic behavior of this solution is representative of all the platinum–ethidium complexes containing an acetate counterion. At the lowest temperature, a 486-nm absorption band predominates and the solution appears orange. As the temperature increases, this band diminishes in intensity with a concomitant increase of the 644-nm absorption band. The presence of isosbestic points (vide infra) indicates that the thermochromism probably results from the simple interconversion of two species.

In order to determine whether a temperature-dependent acid/base equilibrium might be responsible for the thermochromism, absorption spectra were recorded in water as a function of pH. The pH-dependent absorption spectra of *cis*-[Pt(NH$_3$)$_2$(*N3*-Etd)Cl](OAc)$_2$, chosen as a representative case, revealed that the orange/blue conversion is indeed pH dependent, with the orange species predominating under acidic conditions (Figure 3). Potentiometric titrations were therefore carried out to quantitate this pH dependence. Because substantial decomposition occurred at pH values greater than 7, as indicated by significant hysteresis in the titration curves, the acidity constants of the Pt–Etd complexes could not be determined by conventional potentiometric analysis. Instead, they were estimated through a global analysis treatment of the thermochromic equilibria, as described below.

Significant enhancement of the acidity of an amino group upon coordination to platinum(II) is well documented.[36] Reversible protonation of the platinum-bound amino groups of *o*-phenylenediamine (OPD) has been reported for the complex [Pt(PPh$_3$)$_2$(*N1*-,*N2*-OPD)]$^{2+}$.[37] In a related compound, *cis*-[Pt(NH$_3$)$_2$(*N9*-9-AA)Cl]$^+$,[23] the enhancement was so dramatic that the coordination of Pt was accompanied by simultaneous proton transfer from *N9* to *N10*. These examples suggest that the spectroscopically observed acid/base equilibrium most likely involves protonation and deprotonation of a platinum-bound exocyclic amino group of the ethidium ligand.

(36) Lippert, B.; Arpalahti, J.; Krizanovic, O.; Micklitz, W.; Schwarz, F.; Trötscher, G. In *Platinum and Other Metal Coordination Compounds in Cancer Chemotherapy*; Nicolini, M., Ed.; Nijhoff: Boston, 1988; p 563.

(37) Pizzotti, M.; Cenini, S.; La Monica, G. *Inorg. Chim. Acta* **1978**, *33*, 161.

In aqueous solution, deprotonation of the platinum–ethidium complexes is effected by hydroxide ion. In alcohol solution, however, where the thermochromism is most pronounced, the proton acceptor is the acetate counterion. As shown in Figure 4, *cis*-[Pt(NH$_3$)$_2$(*N3*-Etd)Cl]Cl$_2$, which has no acetate acceptor, does not exhibit thermochromic behavior in solution. When potassium acetate was added to this solution, however, the thermochromic behavior was restored (data not shown), demonstrating that acetate anion serves as the proton acceptor in the thermochromic systems. A schematic representation of this chemistry is illustrated in eq 2.

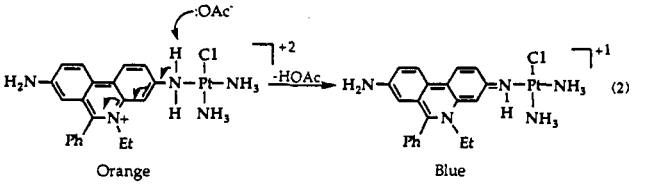

(2)

Thermodynamic parameters for the thermochromic equilibria were derived in the following manner. For a given Pt–Etd complex dissolved in a polar solvent such as methanol, the equilibrium responsible for the color change is written as indicated in eq 3.

$$\underset{C_0(1-x)}{[OR]} + \underset{C_0(n-x)}{OAc^-} \rightleftharpoons \underset{C_0x}{[BL]} + \underset{C_0x}{HOAc} \qquad (3)$$

For convenience, the protonated and the deprotonated forms are denoted as [OR] and [BL], respectively. In this equation, n is the number of acetate counterions, C_0 is the total platinum concentration, and x is the mole fraction of [BL] formed. An equilibrium expression for this reaction is given by eq 4, the

$$K = \frac{x^2}{(1-x)(n-x)} \rightarrow (1-K)x^2 + (1+n)Kx - nK = 0 \qquad (4)$$

nontrivial solution of which is shown in eq 5. The absorbance at any given wavelength, $A(\lambda)$, can be expressed as the sum of the contributions of the orange and blue forms, eq 6. From the

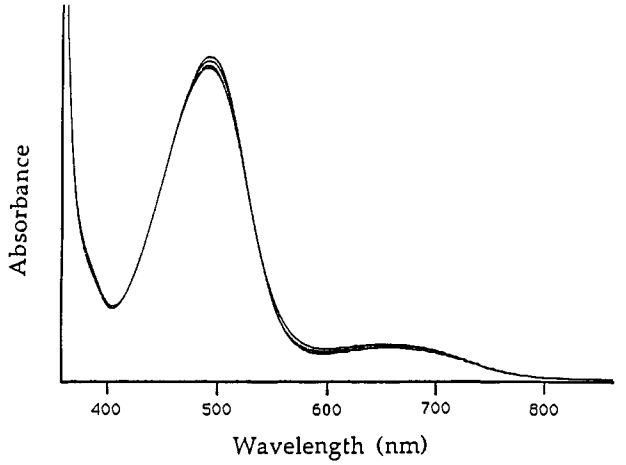

Figure 4. Optical absorption spectrum of *cis*-$[Pt(NH_3)_2(N3\text{-Etd})Cl]Cl_2$ (**1c**) in MeOH between 25 and 50 °C.

$$x = \frac{2nK}{(n+1)K + \sqrt{(n-1)^2K^2 + 4nK}} = \frac{2n}{(n+1) + \sqrt{(n-1)^2 + \frac{4n}{K}}} \quad (5)$$

$$A(\lambda) = xA_{BL} + (1-x)A_{OR} \quad (6)$$

equilibrium constants obtained from eq 5, the thermodynamic parameters $\Delta H°$ and $\Delta S°$ can be derived according to the standard relationships given in eq 7. The system is defined by four

$$K = \exp(-\Delta G°/RT) = \exp(-\Delta H°/RT)\exp(\Delta S°/R) \quad (7)$$

parameters, A_{BL}, A_{OR}, $\Delta H°$, and $\Delta S°$. The first two are wavelength dependent and the latter are global parameters, that is, imposed by the model at all wavelengths.

On the basis of the above algorithm, we have successfully fit the measured spectra for complexes **1a**, **2a**, **2b**, **4a**, and **4b** by global analysis. Complexes **1b**, **3a**, and **3b** were not treated owing to their very limited optical density changes within the accessible temperature range (–50 to 50 °C). Initial guesses for $\Delta H°$ and $\Delta S°$ were crucial for proper convergence of the global fitting procedure. This problem was solved by using $\Delta H°$ and $\Delta S°$ values obtained from a least-squares analysis of the temperature dependence at a single wavelength in the vicinity of an absorption maximum. Such a single curve analysis at 640 nm is shown for compound **4b** in Figure 5.

Plots of the measured spectra and the fits obtained for compound **4b** at various temperatures are presented in Figure 6. The calculated spectra of both the [BL] and [OR] forms of this complex, obtained by using the derived A_{BL} and A_{OR} values defined in eq 3, are shown in Figure 7. Overlay plots and extracted spectra of this kind for compounds **1a**, **2a**, **2b**, and **4a** are provided as supplementary material (Figure S1–8). In most cases, the agreement between the experimental data and the theoretical fit is satisfactory, judging by the shape of the extracted spectra for the orange and blue limiting species. The quality of the fits, however, can also be evaluated by comparing the thermodynamic parameters $\Delta H°$ and $\Delta S°$ derived from two independent spectral data sets for each compound (Table IV). For **2a** and **4b** the fits obtained in two independent sets of measurements are in good agreement. On the other hand, larger deviations occur for **1a**, **2b**, and **4a**. In addition, negative absorption, which is physically unreasonable, appeared in the extracted spectra of **1** and **3** (supplementary material). Small residual peaks were also present in the extracted [OR] spectrum for both **2a** and **4a**.

To identify the source of these errors, the mole fraction (x) values were calculated by eq 5 and the $\Delta H°$ and $\Delta S°$ values

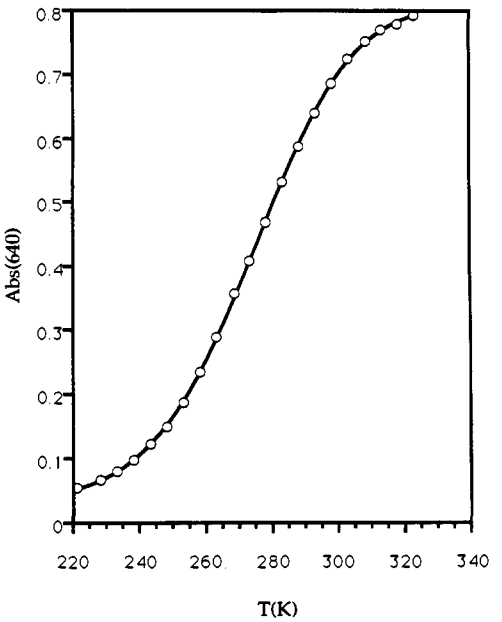

Figure 5. Analysis of the temperature dependence of the absorption spectrum of $[Pt(NH_3)_3(N8\text{-Etd})Cl](OAc)_3$ (**4b**) between –50 and 50 °C at a single wavelength (640 nm). The solid line is the best least-squares fit of the points to the equations given in the text.

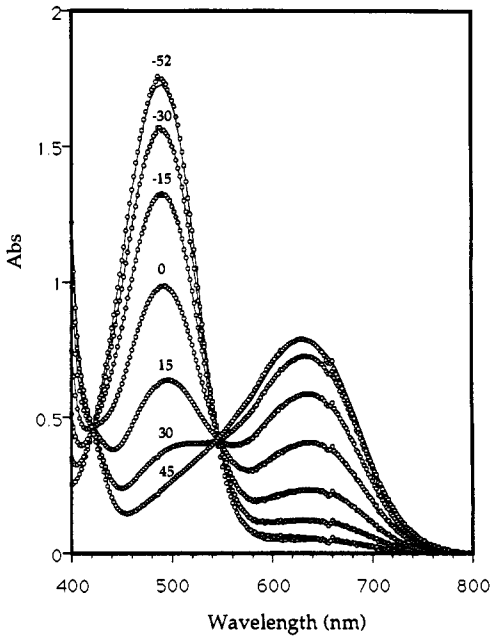

Figure 6. Observed (open circles) and calculated (solid lines) temperature-dependent absorption spectra for $[Pt(NH_3)_3(N8\text{-Etd})](OAc)_3$ (**4b**) in MeOH. Temperatures (°C) are indicated above each curve.

obtained from the fits for all the complexes studied, and the results were plotted as a function of temperature over the entire range (–50 to 50 °C, Figure 8). As can be seen from this figure, the mole fraction is a sigmoidal function of the temperature, varying from 0.035 to 0.973 for **4b** (solid line) and from 0.049 to 0.985 for **2a** (dashed line). On the other hand, x starts at 0.245 (–50 °C) for **4a** and only reaches values of 0.489 and 0.521 at 50 °C for **1** and **3**, respectively. The best agreements between experiment and theory were obtained with compounds for which the mole fraction varies by more than 0.9 over the experimental temperature range. For compounds like **1a** and **2b**, however, a small measurement error at the highest temperature produces considerable uncertainty of the values of both $\Delta H°$ and $\Delta S°$.

Another possible source of error is that, owing to the high acidity of some Pt–Etd complexes studied, an indeterminate amount of acetic acid may be lost during the lyophilization step,

Table IV. Thermodynamic Data for Pt–Etd Complexes

	R^a	$\Delta H°$ (kcal/mol)^c	$\Delta S°$ (eu)^c	$K_{298.15}{}^c$	K_a(MeOH)^d	$K_a(H_2O)^e$	pK_a
cis-[Pt(NH$_3$)$_2$(*N3*-Etd)Cl](OAc)$_2$							
I	1.81	14.19	41.61	0.049	5.49×10^{-8}	5.09×10^{-9}	8.3
II	2.15	13.19	37.20	0.029	3.25×10^{-8}	3.02×10^{-9}	8.5
trans-[Pt(NH$_3$)$_2$(*N8*-Etd)Cl](OAc)$_2$							
I	2.38	13.11	36.23	0.020	2.24×10^{-8}	2.08×10^{-9}	8.7
II	2.20	11.88	34.88	0.083	9.30×10^{-8}	8.63×10^{-9}	8.1
trans-[Pt(NH$_3$)$_2$(*N3*-Etd)Cl](OAc)$_2$							
I	2.04	15.51	56.31	8.69	9.73×10^{-6}	4.92×10^{-7}	6.3
II	2.86	14.92	52.80	3.99	4.47×10^{-6}	4.15×10^{-7}	6.4
[Pt(NH$_3$)$_3$(*N8*-Etd)](OAc)$_3$							
I	2.90	15.20	52.72	2.39	2.68×10^{-6}	5.10×10^{-8}	7.3
free fit	0.07[b]	15.48	53.61	2.32	2.60×10^{-6}	4.95×10^{-8}	7.3
II	2.95	14.53	49.76	1.67	1.87×10^{-6}	3.56×10^{-8}	7.5
free fit	0.03[b]	14.71	50.36	1.66	1.86×10^{-6}	3.54×10^{-8}	7.5
[Pt(NH$_3$)$_3$(*N3*-Etd)](OAc)$_3$							
I	3.42	16.00	63.55	144.5	1.62×10^{-4}	3.08×10^{-6}	5.5
II	3.10	13.18	52.06	52.4	5.87×10^{-5}	1.11×10^{-6}	6.0

[a] R = Int(OAc)/Int(Etd) from the ^{1}H NMR. [b] α, the deviation from exact stoichiometric ratio (3). [c] Determined by the global analysis algorithm (see text for details). [d] Calculated according to eq 8. [e] Estimated by eq 9.

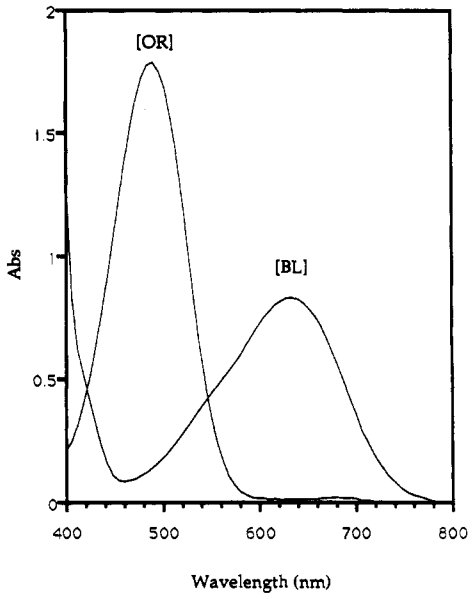

Figure 7. Spectra derived from the global analysis for the two chromophores of [Pt(NH$_3$)$_3$(*N8*-Etd)](OAc)$_3$ (**4b**) corresponding to the two temperature, or pH, limits of the titration.

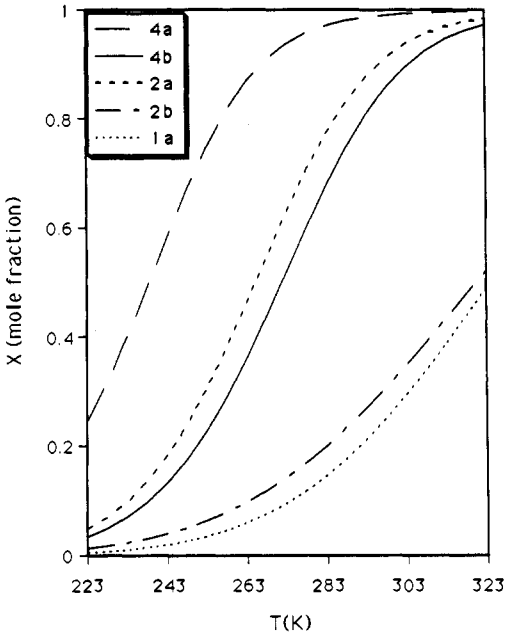

Figure 8. Temperature dependence of the mole fraction for Pt–ethidium complexes; see inset for legend.

producing some of the corresponding blue species in the solid state. It is alternatively possible that excess acetic acid was trapped in the lattice. To control for these errors, the true ratio (R) of platinum complex cation to acetate anion was quantitated by comparing the intensity of the methyl protons of ethidium with that of the methyl protons of acetate in the NMR spectra of the complexes. The results are included for each sample in Table IV. In an attempt to account for these small deviations from the expected stoichiometric ratio, additional calculations were carried out in which a parameter α, the deviation from ideal stoichiometry, was incorporated into the algorithm, as detailed in an appendix supplied in the supplementary material. Owing to the high nonlinearity of the algorithm, the success of this approach was limited to the spectral data of compound **4b**. Values of the parameters obtained by this treatment are also provided in Table IV for comparison.

By rewriting eq 4 in the manner given by eq 8, one can readily calculate the acidity constant of the Pt–Etd complexes, K_a(Pt),

$$K = \frac{[BL][HOAc]}{[OR][OAc^-]} = \frac{[BL][H^+]}{[OR]} \frac{[HOAc]}{[OAc^-][H^+]} = K_a(Pt)/K_a(HOAc) \quad (8)$$

in MeOH from the equilibrium constant K derived from global analysis of the thermochromic equilibrium and the known K_a value for acetic acid in MeOH, 1.12×10^{-6} at 25 °C.[38] In addition, the pK_a(Pt) value in H_2O at 25 °C can be estimated from that in methanol by using the relationship of eq 9.[38] Details are

$$\log \frac{K_a(MeOH)}{K_a(H_2O)} = \frac{2.409}{r}(2n - 1) \quad (9)$$

provided in the appendix supplied with the supplementary material. In eq 9, r is the radius of the acid, approximately 7 Å for a typical Pt–Etd complex as determined by examining a molecular model, and n is the charge on the acid. Since the Pt–Etd complexes do not satisfy the assumption made in deriving eq 9 that the acid is spherical, the acidity constant in aqueous solution is at best an approximation.

Table IV summarizes the acidity constants determined in this manner, from which three interesting trends emerge. First, the *N3* linkage isomers are more acidic than their *N8* analogues, with pK_a values that are lower by about 1.5 units. We attribute this difference to the fact that the electron density generated by

(38) Kucharsky, J.; Safarik, L. *Titrations in Non-aqueous Solvents*; Elsevier: Amsterdam, 1965.

the removal of the proton can be better delocalized over the phenanthridium ring for an *N3* isomer compared to the corresponding *N8* isomer. A similar argument was invoked in a study of the 3-amino- and 8-amino-5-ethyl-6-phenylphenanthridinium ion, where it was concluded that the energy difference between the two most stable resonance structures of the two isomers was too small to be detected spectroscopically.[34,39] The present results provide evidence of this energy difference through a more sensitive probe, the acidity of the exocyclic amino group.

The second finding is that *trans*-$[Pt(NH_3)_2(N3\text{-Etd})Cl](OAc)_2$ is about 2 pK_a units more acidic than the corresponding cis isomer. This thermodynamic trans effect seems reasonable, since the more electron releasing ammine ligand in the trans position (cis isomers) would destabilize the deprotonated form of the ethidium ligand. Thus, the imino bond generated by deprotonation of the exocyclic amino group is more stable with a chloride ligand in the trans position than an amine.

The third observation is that auxiliary ligands in the platinum coordination sphere also affect the relative acidity of the coordinated exocyclic amino group. In methanol solution, both *N8* and *N3* linkage isomers of $[Pt(NH_3)_3(Etd)]^{3+}$ are more acidic than their corresponding $[Pt(NH_3)_2(Etd)Cl]^{2+}$ analogues. The greater acidity of the triamine complexes is a consequence of their higher effective positive charge on the Pt center. The difference in acidity, however, is reduced in aqueous solution. This result reflects the fact that a more highly charged ion is better stabilized in a solvent of greater dielectric constant, thus diminishing the thermodynamic driving force for its deprotonation.[38]

Another interesting property which is influenced by the effective charge on the complex is that, although all the Pt–Etd compounds studied are weaker acids than acetic acid in aqueous solution, compounds **2a**, **4a**, and **4b** are more acidic than acetic acid in methanol.

MO Analysis of the Electronic Structures of Pt–Etd Complexes. The Fenske–Hall methodology[19] was employed to investigate the electronic structures of the Pt–Etd complexes, to analyze differences among them, and to assign the optical transitions responsible for the [OR] and [BL] chromophores. As described in the Experimental Section, methidium (Mtd) was used in place of Etd to simplify the calculations. For the [OR] forms, the geometric parameters involving the Pt center were readily available from the crystallographic results for **1c** and **1d**. For the [BL] form, however, the orientation of the Mtd plane relative to the Pt-coordination plane was critical in determining the HOMO-LUMO gap. The most reasonable results were obtained by using the dihedral angle previously reported for *cis*-$[Pt(NH_3)_2(N9\text{-}9\text{-aminoacridine})Cl]^{2+}$.[23] Because of the low symmetry (C_1) of the model compounds used in the calculations, extensive mixing occurs among orbitals from nonbonded atoms in almost every calculated MO. Moreover, most of the occupied MO's are those predominantly involved in Mtd (C–C, C–N, C–H and N–H) σ- and (C–C and C–N) π-bonding interactions, which are energetically distant from the frontier orbitals. An exhaustive investigation of this entire set of molecular orbitals was therefore not attempted in the interest of time and relevance. Rather, MO's for the [OR] and [BL] forms of model **1** were analyzed in detail in order to gain insight into the factors responsible for the solution thermochromism of this compound. The results of this analysis were then used to evaluate models for compounds **2**, **3**, and **4** and, in particular, to reveal any differences from **1**. Table S13 (supplementary material) summarizes our findings for the four model compounds, including the relative energies, atomic orbital contributions, and assignments of the dominant contribution for the upper valence molecular orbitals.

***cis*-$[Pt(NH_3)_2(N3\text{-Mtd})Cl]^{2+}$.** An interesting splitting pattern in the Pt d orbitals is readily apparent for the protonated [OR] form of this complex (an orbital energy level diagram is provided in Figure 9). The d_{yz} (No. 68) orbital is the least perturbed because of the lack of a π-type orbital on either *N3* or the NH_3 group trans to *N3*, and its energy level is therefore close to that of the d orbital of the free Pt^{2+} ion; both d_{xz} (No. 64) and d_{xy} (No. 66) are stabilized relative to the free ion through a bonding interaction with the lone pairs of the Cl atom; d_{z^2} (No. 69) is destabilized by σ donation from both Cl and N3 and thus becomes the highest occupied d orbital; and $d_{x^2-y^2}$, the only empty d orbital, is of very high energy since it is the antibonding component of a molecular orbital set used in metal–ligand σ bonding. The list of the d-block orbitals in the order of ascending energy is therefore $d_{xz} < d_{xy} < d_{yz} < d_{z^2} \ll d_{x^2-y^2}$. The HOMO is a pair of pseudodegenerate orbitals (Nos. 71, 72) of dominant Cl lone pair character, whereas the SHOMO (second highest occupied MO) is the lone pair orbital of *N8* (No. 70) and lies only 0.6 eV below the HOMO pair. The LUMO orbital (No. 73) is the π^* orbital of the phenanthridium group and is 5.22 eV above the HOMO.

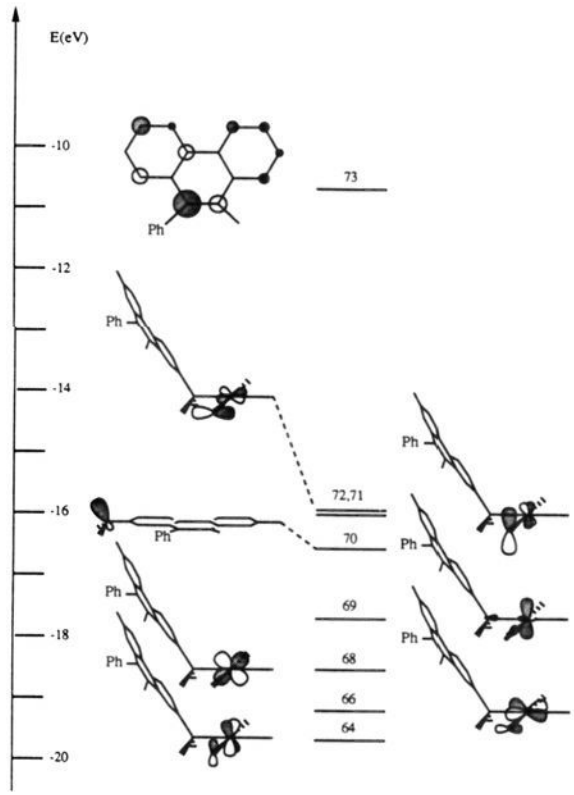

Figure 9. Orbital and energy level diagram of the [OR] form of *cis*-$[Pt(NH_3)_2(N3\text{-Mtd})Cl]^{2+}$.

The frontier orbitals and all the Pt-based orbitals for the deprotonated [BL] form of **1** are also listed in Table S13 (supplementary materials) and an energy level diagram is provided in Figure 10. The order of the d-block, d_{xz} (No. 65) ~ d_{xy} (No. 66) < d_{yz} (No. 68) < d_{z^2} (No. 69) ≪ $d_{x^2-y^2}$ (No. 80), is very similar to that of the [OR] complex, but a significant change occurs in the metal–ligand interactions as a result of many in- and out-of-phase mixings between d_{xy} and the $\pi(\pi^*)$ orbitals of the phenanthridium ring. The pseudodegenerate HOMO pair in the [OR] complex is split in the [BL] form by the antibonding contribution from *N3* (18%) to MO No. 72, which is 0.63 eV above the SHOMO (No. 71). In addition the lone pair from *N8* (No. 67), the SHOMO in [OR], is far below the HOMO (3.28 eV). Although the same π^* orbital of Mtd remains as the LUMO, the HOMO-LUMO gap is reduced to 3.73 eV, which is 1.49 eV smaller than the corresponding energy separation in [OR].

***cis*-$[Pt(NH_3)_2(N8\text{-Mtd})Cl]^{2+}$.** The energy level and charge distributions of the valence MO's are essentially the same as for

(39) Zimmermann, I.; Zimmermann, H. W. *Ber. Bunsen-Ges. Phys. Chem.* **1976**, *80*, 991.

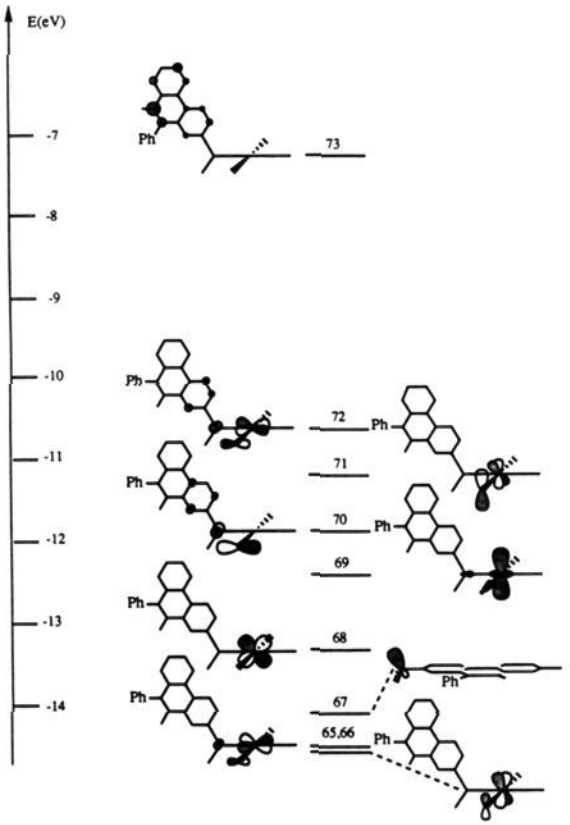

Figure 10. Orbital and energy level diagram of the [BL] form of *cis*-$[Pt(NH_3)_2(N3\text{-Mtd})Cl]^{2+}$.

the *N3* linkage isomer. The HOMO-LUMO gaps are 4.91 and 3.38 eV for the [OR] and [BL] forms, respectively.

***trans*-$[Pt(NH_3)_2(N8\text{-Mtd})Cl]^{2+}$.** The valence MO's are very similar to those of *cis*-$[Pt(NH_3)_2(N8\text{-Mtd})Cl]^{2+}$. The only difference is that the order of the d_{xz} and d_{yz} orbitals has been inverted, owing to the trans disposition of the Cl atom. The HOMO-LUMO gaps are 4.24 and 3.26 eV for the [OR] and [BL] forms, respectively.

$[Pt(NH_3)_3(N8\text{-Mtd})]^{3+}$. Because there is no π-donor (acceptor) ligand, the d-orbital splitting pattern in the [OR] form of this complex is that of a typical square-planar complex, d_{xz} (No. 63) $\sim d_{yz}$ (No. 64) $< d_{xy}$ (No. 65) $< d_{z^2}$ (No. 66) $\ll d_{x^2-y^2}$. A dramatic difference between this result and those discussed above is that the lone pair on *N3* becomes the HOMO. The π^* orbital of the ring, lying 4.82 eV above the HOMO, remains the LUMO.

In the [BL] form the HOMO is a pure π-antibonding orbital distributed among *N8*, Pt, and the phenanthridium ring. The lone pair from *N3* is 1.62 eV below the HOMO. The HOMO-LUMO gap (4.56 eV) is very close in energy to, although smaller than, the one obtained for the [OR] form.

Assignment of Optical Transitions. From the foregoing description of the upper valence orbitals, it is clear that the HOMO-LUMO transition is responsible for the visible band in the [OR] form of the $[Pt(NH_3)_3(N8\text{-Etd})]^+$ cation. This transition corresponds to charge transfer from the lone pair of *N3* to the π^* orbital of the phenanthridium ring. The assignment is supported by the fact that the SHOMO is about 3 eV below the HOMO; the latter is therefore the only reasonable donor orbital. This assignment also agrees with a previous analysis of the electronic spectrum of free ethidium.[40]

On the other hand, unambiguous assignments of the optical transitions in the visible region for all $[Pt(NH_3)_2(Etd)Cl]^{2+}$ complexes are not directly available from the results presented above because of the small energy difference (0.6 to 1.3 eV) between the SHOMO and HOMO. It is noteworthy that the absorption maxima for the [OR] forms of all the complexes occur at ~480 nm with similar extinction coefficients. This result suggests that an identical transition is responsible for this band in all the isomers. Furthermore, since there is little charge density on the portion of the phenanthridium ring near the coordinated exocyclic amino group in the LUMO, direct overlap between the LUMO and the HOMO is negligible if not identically zero. The HOMO-LUMO transition is therefore expected to be very weak,[41] and less likely to be responsible for the absorption at 480 nm, which has an extinction coefficient of *ca.* 8×10^3 M^{-1} cm^{-1}. We therefore assign the visible band in these complexes to the SHOMO-LUMO transition.

The absorption in the visible spectral region for all the deprotonated [BL] forms can no longer be attributed to charge transfer between the lone pair of the free exocyclic amino group and the π^* orbital of the ring, since the former is far below the HOMO ($\Delta E > 3.3$ eV for **1**, **2**, and **3**, and $\Delta E = 1.6$ eV for **4**). Instead, the band appears more likely to involve charge transfer from the HOMO, and possibly also the SHOMO, to the LUMO. Such an assignment is based on the fact that the HOMO of all [BL] complexes contains significant contributions (~20%) from both the p_π orbital of the coordinated amine and the p_π orbitals of C1, C2, and C4. A significant transition dipole moment is therefore expected.

Thus, deprotonation shifts the donor orbital involved in charge transfer from the uncoordinated to the coordinated exocyclic amino group of the ethidium ligand, now a major contributor to the HOMO, the acceptor (LUMO) remaining the π^* orbital of the ring in both cases. From the discussion above it is evident that the HOMO-LUMO gaps for [BL] complexes are always smaller than the SHOMO-LUMO gaps in the corresponding [OR] forms, which accounts for the observed red shift of the absorption maximum upon deprotonation.

It should be pointed out that, despite the consistency in the qualitative assignments just made, none of the calculated (S)HOMO-LUMO gaps matches the experimentally determined transition energies (orange forms at 480 nm, ca. 2.58 eV; blue forms, 640 nm, ca. 2.06 eV). The difference between the transition energies of the [OR] and [BL] forms also does not correspond quantitatively to the observed red-shift of ca. 0.5 eV. These discrepancies are not unexpected, however, since it is well-known that the single Slater determinant Hartree–Fock method tends to overestimate the Coulombic repulsion of the unoccupied orbitals, and consequently a larger HOMO-LUMO gap is always found in such calculations.[42] In addition, we have not been able to correlate the results of the present MO calculations with the observed trend in the acidity of the Pt–Etd complexes, which is not surprising since acidity has rarely been addressed by SCF-MO methods.

***Effect of DNA on the Linkage Isomer Obtained during* Formation of a Ternary Complex among Ethidium, Platinum, and a Nucleobase.** As previously reported, DNA can serve as a template to facilitate the reaction of *cis*-DDP and ethidium to form ternary ethidium–Pt–DNA complexes.[5-7] The nature of these complexes was revealed when it was demonstrated that covalent binding of *cis*-$[Pt(NH_3)_2(N3\text{-Etd})Cl](OAc)_2$ and *cis*-$[Pt(NH_3)_2(N8\text{-Etd})Cl](OAc)_2$ to DNA affords species which are spectroscopically indistinguishable from ternary complexes formed by addition of *cis*-DDP and ethidium to DNA.[7] The ternary complexes therefore consist of a $\{Pt(NH_3)_2\}^{2+}$ moiety covalently bonded to the 3-amino (or 8-amino) group of ethidium as well as to the *N7* position of a purine nucleobase. Remarkably, the reaction rate of platinum with the ethidium exocyclic amino group is much more rapid in the presence of DNA than in its

(40) Le Bret, M.; Chalvet, O. *J. Mol. Struct.* **1977**, *37*, 299.

(41) Ballhausen, C. J. *Molecular Electronic Structures of Transition Metal Complexes*; McGraw-Hill: London, 1979.

(42) Connolly, J. W. D. In *Semiempirical Methods of Electronic Structure Calculation. Part A: Techniques*; G. A. Segal, Ed.; Plenum Press: New York, 1977.

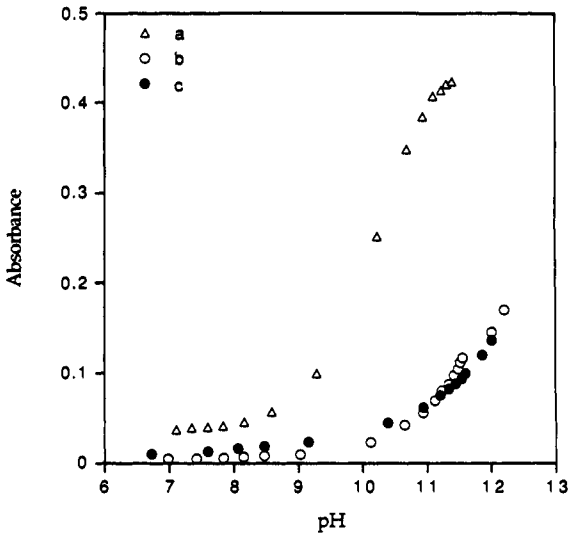

Figure 11. Plot of absorbance versus pH for (a) *cis*-[$Pt(NH_3)_2$(*N3*-Etd)]–calf thymus DNA, (b) *cis*-[$Pt(NH_3)_2$(*N8*-Etd)]–calf thymus DNA, and (c) Pt–Etd–calf thymus DNA ternary complex generated in situ. R_f is 0.1. The absorbances were monitored at 612 nm.

absence. Possibly, the DNA double helix serves both to increase the collision frequency of the freely diffusing Etd^+ moiety with the covalently anchored *cis*-diamminechloroplatinum(II) fragment and to orient the two reagents, optimizing the stereochemistry required for nucleophilic displacement of the chloride ion. If this model is correct, then DNA might also be expected to influence the regioselectivity of the reaction of *cis*-diamminechloroplatinum(II) with ethidium. In particular, our previous model building studies suggested that platinum might react preferentially at the *N8* rather than the *N3* position of the phenanthridium ring.[7]

Until now, however, it has not been possible to assess the regioselectivity of this DNA-promoted reaction because the absorption spectra of ternary complexes formed by the *N3* and *N8* isomers are nearly identical.[7] The discovery that the different linkage isomers have distinctly different pK_a values, however, provides a spectroscopic means of assessing which amino group of the ethidium ion is coordinating to platinum in the DNA-promoted reaction. As shown in Figure 11, the color change that accompanies deprotonation of the platinated exocyclic amino group in the *cis*-$\{Pt(NH_3)_2$(*N3*-Etd)$\}^{3+}$ and *cis*-$\{Pt(NH_3)_2$(*N8*-Etd)$\}^{3+}$ DNA adducts occurs at a much lower pH value for the former than the latter. This result nicely parallels the relative pK_a values of the corresponding chloro complexes of these two cations. Moreover, the figure reveals that the titration curve for the ternary complex closely mimics that for the adduct made with the *N8* isomer. These data indicate that the reaction of *cis*-DDP and ethidium on a DNA template is regiospecific, with platinum reacting at the *N8*-amino position of ethidium. This regiospecificity reflects the asymmetric binding of Etd with respect to the pseudo-2-fold axis that passes between adjacent base pairs of the double helix.[7,43,44] Thus, DNA serves not only to increase the reaction rate of cisplatin with Etd but also to direct the reaction to the *N8* exocyclic amino group. This result provides the first example of regiospecificity in a DNA-promoted reaction, further supporting the concept that the double helix serves to bind and orient the two reactants in much the same manner as occurs in enzyme-catalyzed condensation reactions.

(43) Tsai, C. C.; Jain, S. C. *J. Mol. Biol.* **1977**, *114*, 317.
(44) Lybrand, T.; Kollman, P. *Biopolymers* **1985**, *24*, 1863.

Concluding Remarks

In this paper we have thoroughly characterized a series of complexes formed between platinum(II) ammines and the ethidium cation. Platinum binding occurs at both exocyclic amino groups of ethidium forming linkage isomers that can be separated chromatographically. The structures of these complexes have been determined for representative examples by X-ray crystallography in the solid state, in solution by NMR spectroscopy, and in the gas phase by mass spectrometry. The orange-to-blue thermochromism of solutions of the acetate salts of the complexes has been shown to arise from deprotonation of the exocyclic amino group to which the platinum atom is coordinated, the presence of the positively charged metal ion at this position lowering the pK_a of this group. The change in pK_a is affected by the overall charge on the complex, the linkage isomer, and the stereoisomer (cis versus trans) in a manner dictated by the electronic properties of the resulting acid anion. From Fenske–Hall molecular orbital calculations it has been possible to assign the visible spectral transition of the orange and blue species. The former arises from charge transfer involving the lone pair on the unplatinated ethidium amino group and the π^* orbital of the ring (LUMO), whereas in the blue complexes, the optical transition is from an orbital (HOMO) localized primarily near the coordinated, now deprotonated, imino functionality to the same acceptor orbital. Finally, the solution thermochromism of these complexes has been used to identify the regiospecificity of the ternary complex formed between *cis*-diamminedichloroplatinum(II), ethidium, and calf thymus DNA. This DNA-promoted reaction leads predominantly to the single regioisomer in which DNA-bound platinum is coordinated to the 8-amino group of the ethidium ring.

Acknowledgment. This work was supported by U.S. Public Health Service Grant CA34992 (to S.J.L.) from the National Cancer Institute and NIH National Research Service Award GM11880-01 from the National Institute of General Medical Sciences (to D.P.B.). A.M. thanks the Human Frontier Science Program Organization for a fellowship and research funding. FAB mass spectra were obtained with the assistance of Dr. C. Costello at the facility supported by NIH Grant RR 00317 (Principal Investigator, Prof. K. Biemann) from the Biotechnology Resources Branch, Division of Research Resources. We also thank Drs. L. Chassot and J. G. Bentsen for helpful discussions.

Supplementary Material Available: Tables of atomic positional parameters for non-hydrogen atoms, anisotropic temperature factors, bond distance and angles, and torsion angles for **1c** and **1d** (Tables S1, 2, 4–8, 10–12), the Appendix, figures of overlay and extracted spectra for complexes **1a**, **2a**, **2b**, and **4a** (Figures S1–8), and tabulation (Table S13) of upper valence molecular orbitals from Fenske–Hall calculations (31 pages); listing of calculated and observed structure factors (Tables S3 and S9) (42 pages). Ordering information is given on any current masthead page.